A Redundant Strapdown Inertial Reference Unit (SIRU)

JEROLD P. GILMORE* AND RICHARD A. MCKERN†
Charles Stark Draper Laboratory
Massachusetts Institute of Technology, Cambridge, Mass.

The hardware and software mechanization of the SIRU redundant strapdown system is described. Six gyroscope and six accelerometer modules are arranged with their input axes in a unique symmetrical pattern that corresponds to the array of normals to the faces of a dodecahedron. This configuration enables optimal data processing with self-contained failure isolation for up to two out of six of either instrument module type, and continued operation with as many as three out of six failures. Each instrument module is a prealigned normalized assembly that contains its own torque-to-balance electronics, temperature controller, etc. The modular features provide enhanced system maintainability. Redundant hardware concepts are applied in the supporting instrumental package electronics (dual-power supplies, triple-redundant clocks, etc.). The degree of redundancy use in the Electronics Assembly is based upon the relative reliability of the individual circuits and circuit isolation concepts. The system has been mechanized so that satisfactory operation is achieved with a variety of electronic and instrument degradation or catastrophic failures and is free from the possibility of a system failure resulting from a single-point failure mechanism. Descriptions of the software data processing and failure isolation algorithms are presented with an itemization of the system's computational real-time and memory requirements.

Introduction

IN recent system applications, attention has been focused on the use of redundancy concepts to achieve a significant improvement in reliability, and thus enhance mission success. In commercial and military aviation, the triplicate usage of individual systems is becoming commonplace. In the Apollo spacecraft, a "primary" system complimented by a "backup" system with limited mission-mode capabilities was employed. For future missions, a "back-up" concept is not considered acceptable since its objective is a fail-safe return and does not enhance mission success. In the case of today's triplicate system implementations, failure isolation and system selection are for the most part operator monitoring and decision functions. Advanced systems will undoubtedly require automatic failure detection and adaptation, especially in guidance phases.

Various choices are possible when one considers instrument and functional redundancy. The basic concept, however, evolves about redundantly employed sensors computationally processed in common orthogonal axes or a nonorthogonal configuration of sensors each possessing a measure of redundant data. In all cases, the redundancy objective is to achieve a mechanization that is free from single-point failure modes and incorporates a self-contained failure detection and adaptation feature. Further, the bandwidth and nature of the detection and adaptation scheme must assure that maximum reliability is achieved, i.e., neither performance degradation nor a failure endangers the proper operation of the system.

The Redundant Strapdown Inertial Reference Unit (SIRU) consists of a Redundant Instrument Package (RIP), an Electronics Assembly (EA), and Digital Computation Assembly (DCA). The RIP is an assembly of six single degree-of-freedom gyroscope modules and six linear accelerometer modules. Each module is prealigned, normalized and includes the instrument, its pulse torque-to-balance electronics, temperature controller, etc. Redundant concepts are also applied in the supporting electronics assembly (power supplies, clock and scalers, etc.).

The module outputs are in the form of an increment of angular motion $\Delta\theta$ and velocity ΔV for the gyro and accelerometer module, respectively. These outputs are processed through the computational structure to attain inertial attitude and velocity.

Geometric redundancy is achieved by using a nonorthogonal mounting configuration in which instrument input axes (IAs) are oriented to correspond to the array of normals to the faces of a dodecahedron, Fig. 1. This yields a unique symmetry in which all instrument IAs are at a spherical angle 2α (63.4°) from each other; pairs of gyro or accelerometer axes lie in the orthogonal planes of the reference triad and are displaced by the angle α from the principal triad axes. This symmetry yields optimal[1] redundant reorganizational data processing with minimum error propagation. Further, by means of instrument-output comparisons, self-contained failure isolation of up to 2 of 6 of both instrument types is achieved, and a third failure may be detected. With the aid of additional diagnostics, the processing structure also allows continued operation with 3 of 6 having failed.

A relative comparison of SIRU reliability with respect to other sensor arrangements is illustrated by comparing each

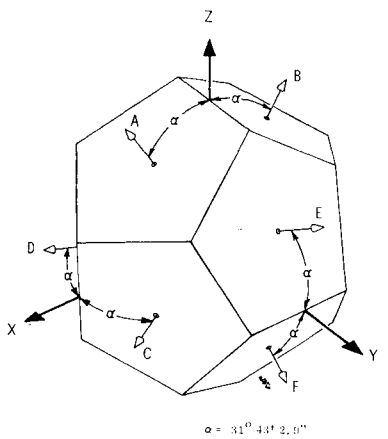

Fig. 1 Instrument input axes orientation relative to the instrument frame triad and the dodecahedron.

Presented as Paper 70-1027 at the AIAA Guidance, Control and Flight Mechanics Conference, Santa Barbara, Calif., August 17–19, 1970; submitted October 13, 1970; revision received September 27, 1971. This work was sponsored by the Manned Spacecraft Center of the NASA through Contract NAS-9-8242.

* Director, Apollo Inertial Subsystems.
† Assistant Director, Systems Analysis. Member AIAA.

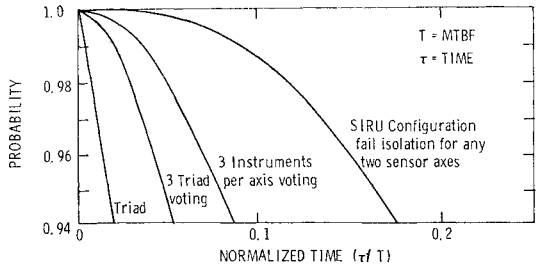

Fig. 2 Mission success probability.

configuration's probability of mission success with time (Fig. 2). In the illustration, all system-sensor axes are assumed to have the same mean-time-before-failure (T). The curves correspond to systems with self-contained failure-isolation features, i.e., three triads (where failure isolation is attained by majority vote), a single triad with three instruments on each axis (with majority agreement per axis), and the dodecahedron array (which allows the failure of any two axes). The curve for a conventional orthogonal triad is also shown for reference purposes. A marked reliability advantage for the SIRU configuration is clearly observable. Further, even if external failure isolation is assumed so that operation continues until all three triad systems fail or a fourth SIRU axis fails, SIRU reliability is 0.999 compared to 0.98 for a normalized time (t/T) of 0.1. With respect to reliability, it is important to note that redundancy itself is not a cure-all. Each element in the system must be selected and conservatively applied in a manner that is consistent with the environment and the mission duration; there is no substitute for quality engineering. Similarly, an element's statistical MTBF of 1,000,000 hr does not preclude its failure, on a random or defect basis. Thus, the system is configured to avoid total failure due to multiple element failures.

A representative engineering model of a Digital Computational Assembly (DCA) was designed to fulfill the processing and strapdown-algorithm system requirements.[2] It is a general-purpose computer with duplex processors, memories and I/O sequencers. It was configured to achieve the system high-reliability requirements and incorporates multiple error checking, single-instruction restart capabilities, micro-programed sequence generation, and the use of a serial time-multiplexed input/output.

System Mechanization Concepts

Redundant Instrument Processing

As a first step, we relate the measurement data derived from the gyros and accelerometers whose input axes are colinear with the dodecahedron vectors A–F, in Fig. 1, to a reference triad. For a gyro set, the orientation yields a relationship between angular-rate inputs (W) about triad axes and the gyro measurements (m) that may be expressed in matrix form in terms of the geometry as

$$\mathbf{m} = \mathbf{H}\mathbf{b} \tag{1}$$

where

$$b^T = [W_X \quad W_Y \quad W_Z]$$

$$m^T = [m_a \quad m_b \quad m_c \quad m_d \quad m_e \quad m_f]$$

$$H^T = \begin{bmatrix} S & -S & C & C & 0 & 0 \\ 0 & 0 & S & -S & C & C \\ C & C & 0 & 0 & S & S \end{bmatrix}$$

$$C = \cos\{[5 + (5)^{1/2}]/10\}^{1/2} \cong 0.851$$

$$S = \sin\{[5 - (5)^{1/2}]/10\}^{1/2} \cong 0.526$$

As seen from the equation, each instrument provides a measure of redundant data, e.g., instruments A, B, C, and D all sense a component of input along the X triad-axis. By algebraic solution of the equations, equivalent triad-axis rate or acceleration solutions can be obtained from any three gyros or accelerometers. Subsequent discussion illustrates that it is possible to isolate up to two failures of either type instrument and to detect a third failure through self-contained instrument output comparisons.

The processing structure used to obtain equivalent triad solutions from the dodecahedron array corresponds to a "weighted least-squares" solution form

$$\mathbf{b}' = (\mathbf{H}^T\Psi^{-1}\mathbf{H})^{-1}\mathbf{H}^T\Psi^{-1}\mathbf{m} \tag{2}$$

where: b′ is defined as the best triad-solution estimate and Ψ^{-1} corresponds to a diagonal 6×6 matrix whose terms represent the individual instrument variances. This solution provides a best estimate where both the geometric properties of the configuration and the individual instrument performance statistics are considered. For the dodecahedron array, the computational implementation allows the selection of the appropriate triad solution in accordance with the operational status of the instruments in that Ψ can be modified to reflect either degraded or failed instrument performance. For efficient computational usage, however, only a "go, no-go" criterion has been implemented. Thus, processing reorganization is achieved by replacement of Ψ^{-1} by a status matrix, λ, in which all diagonal elements are unity when all instruments perform satisfactorily. By setting the appropriate elements to zero when failures are detected, a least-squares triad solution can be defined for any combination of instruments (i.e., 5-, 4-, and 3-gyro or accelerometer combinations). In the actual computer mechanization, this is implemented by storage of common parametric elements that are asembled to form the appropriate least-squares solution based on the status of the instruments, λ. This structure is regenerative in that, if instrument "healing" is observed in the failure-isolation process, the instrument may be reinstated. Thus, the failure-isolation criteria enables adaptive data processing. In addition, external monitors may be used to provide additional λ status data to allow continued operation with as many as three gyro or three accelerometer axes failures. It should be noted that a study to continuously develop a weighted least-square estimate in an adaptive fashion has been conducted.[3]

In comparison, a system employing duplex-instrument redundancy on orthogonal axes experiences total failure for two gyro or two accelerometer failures on the same axis, and self-contained isolation of degradation between two instruments on the same axis is not possible. Even triple-orthogonal redundancy, which can achieve failure isolation by instrument voting, is limited by a dual failure on the same axis.

In principle, any six-instrument skewed configuration possesses similar redundant measurement and failure-isolation capabilities. The advantage of the dodecahedron array results from its unique symmetry, whereby the six measurement axes are spherically distributed with equal angles between all axes. This feature minimizes geometric-error amplification, simplifies failure isolation and is optimum where equal likelihood of performance is required in a triad reference frame.

The relative performance of the SIRU configuration for various failure conditions may be put in perspective by comparing the SIRU reference-triad solution statistics to corresponding statistics for an operational three-axis system. In both cases, all instrument axes are assumed to have identical and independent measurement-error characteristics (σ). The three-axis system's (no failures) statistical performance characteristics are then defined as having a standard measurement deviation of σ along any axis with a total three-

dimensional RSS measurement deviation of $(3)^{1/2}\sigma$. In comparison, when all six axes of SIRU are operational, the error statistics of its triad solution are better (triad axis and RSS system deviations of 0.707σ and $(1.5)^{1/2}\sigma$, respectively). Similarly, deviations for the SIRU triad-solutions for the various five-, four-, and three-instrument combinations may also be compared to the basic triad's statistics. These combinations represent SIRU performance, with failed instruments detected and isolated, i.e., the failed axes no longer being used in the triad-solution processing.

In general, a nonorthogonal array's error-propagation with instruments deleted is such that its triad-solution performance statistics reflect both the reduction in measurement data and the deterioration in geometry. Thus, dependent on the geometric positions of the deleted (failed) axes, the solution tends to have a maximum deviation along a specific axis (worst case) and similarly, different failure combinations have more pronounced RSS error amplification than others. However, as illustrated in Table 1 SIRU error propagation is bounded and performance is not significantly effected by processing with reduced instruments.

The first column of Table 1 corresponds to the SIRU processing status, i.e., operation with all instruments, down to combinations of three-instrument axes. For each of these states, the table shows the SIRU worst-case, single-axis, triad-solution deviation and the ratio of the SIRU solution RSS deviation to an equivalent triad-system RSS deviation. Note that SIRU performance with one failure is statistically better than an unfailed triad system and for all two-failure and eight three-failure combinations performance is essentially identical to an unfailed triad. For the remaining worst three-failure combinations, the maximum single-axis solution standard deviation in comparison to a good triad-axis deviation degrades by a factor of three. Similarly, over all RSS performance degrades by a factor of two.

Failure Isolation

A self-contained failure-isolation algorithm that could be used to establish the λ status is based upon a simple comparison of measurement ouputs. The unique symmetrical properties of the array allows one to generate a series of 15 equations (parity equations, Table 2) based on comparison of four measurements. All the equations will have a zero output if all measurements are correct. (In the case of the gyros, each term in the equation corresponds to an accumulated $\Delta\theta$ count over some comparison interval.) If, however, the gyro along A has malfunctioned, Eqs. 1–10 indicate incorrectly, while 11–15 zero, thereby, isolating the failure. If a second instrument failure occurs, inspection of the remaining Eqs. 11–15 would allow another level of failure isolation. If a third failure occurs and none of the equations are satisfied, the failure is detected, but not isolated.

Another technique, which has been synthesized in the computational software, is based on the use of best-estimate solution b', (Eq. 2). For example, the best estimate of what the instrument measurements should be is

$$\mathbf{m}' = \mathbf{H}'\mathbf{b}' \tag{3}$$

Table 1 SIRU performance with instrument failures versus an operational triad system

Instrument failures	Standard deviation (worst-case axis solution)	Ratio of deviation (SIRU solution to a 3-axis system)
None	0.707σ	0.707
1 (6 combinations)	0.927σ	0.816
2 (15 combinations)	1.349σ	1.000
3 (A—8 combinations)	1.349σ	1.178
3 (B—12 combinations)	2.890σ	1.903

Table 2 SIRU parity equations

No.	Instruments	Equation
1	$ABCD$	$(W_A - W_B)C + (W_C + W_D)S = \lvert\varepsilon\rvert$
2	$ABCE$	$(W_B - W_C)C - (W_A + W_E)S = \lvert\varepsilon\rvert$
3	$ABCF$	$-(W_A + W_C)C + (W_B + W_F)S = \lvert\varepsilon\rvert$
4	$ABDE$	$-(W_A + W_D)C + (W_B + W_E)S = \lvert\varepsilon\rvert$
5	$ABDF$	$(W_B - W_D)C - (W_A + W_F)S = \lvert\varepsilon\rvert$
6	$ABEF$	$(W_E + W_F)C - (W_A + W_B)S = \lvert\varepsilon\rvert$
7	$ACDE$	$(W_D - W_E)C + (W_A - W_C)S = \lvert\varepsilon\rvert$
8	$ACDF$	$(W_C - W_F)C + (W_A - W_D)S = \lvert\varepsilon\rvert$
9	$ACEF$	$(W_A - W_F)C + (W_C - W_E)S = \lvert\varepsilon\rvert$
10	$ADEF$	$(W_A - W_E)C + (W_D - W_F)S = \lvert\varepsilon\rvert$
11	$BCDE$	$(W_C + W_E)C - (W_B + W_D)S = \lvert\varepsilon\rvert$
12	$BCDF$	$-(W_D + W_F)C + (W_B + W_C)S = \lvert\varepsilon\rvert$
13	$BCEF$	$(W_B - W_E)C - (W_C + W_F)S = \lvert\varepsilon\rvert$
14	$BDEF$	$(W_B - W_F)C - (W_D + W_E)S = \lvert\varepsilon\rvert$
15	$CDEF$	$(W_C - W_D)C + (W_E - W_F)S = \lvert\varepsilon\rvert$
	$C = \cos(\alpha)$	$S = \sin(\alpha)$ ε = Threshold level

A comparison of the actual measurement (m) with the estimated measurement yield an estimate of the measurement error for all six instruments (E_0').

$$\mathbf{E}_0' = \mathbf{m} - \mathbf{m}' = \mathbf{m} - \mathbf{H}\mathbf{b}' \tag{4}$$

where

$$\mathbf{E}_0'^T = [E_a' E_b' E_c' E_d' E_e' E_f']$$

For example, the estimated error in the measurement of the A-axis instrument is

$$E_a' = \tfrac{1}{2}[m_a - (0.2)^{1/2}(m_b - m_c - m_d + m_e + m_f)] \tag{5}$$

The corresponding measurement-error variance (TSE_0) of the six instruments is

$$TSE_0 = \mathbf{E}_0'\mathbf{E}_0'^T = \mathbf{E}_a'^2 + \mathbf{E}_b'^2 + \mathbf{E}_c'^2 + \mathbf{E}_d'^2 + \mathbf{E}_e'^2 + \mathbf{E}_f'^2 \tag{6}$$

If no instrument errors exist, both equations reduce to zero. If an instrument failure occurs, the error propagates through both Eqs. 5 and 6. It is dominant in the faulty instrument's error estimate, but is also reflected at reduced magnitude in the other instrument-error estimates. If one knew which instrument were at fault and adapted the processing structure, the corresponding five-instrument variance (TSE_j) with the faulty instrument omitted would then equal zero. It can be shown that the relationship between TSE_j, the faulty instrument error E_j', and the TSE_0 is

$$TSE_j = TSE_0 - 2\,(E_j')^2 \tag{7}$$

Thus (from Eq. 7), if a failure exists, the estimate of the failed instrument's squared error corresponds to 50% of the total six-instrument variance (TSE_0).

Detection of a second failure (k) is achieved in a similar manner. Its error estimate E_{jk} is derived using the corrected processing, i.e., the instrument (j) previously failed is not used, and corresponds to

$$TSE_{jk} = TSE_j - 2.5\,(E_{jk}')^2 \tag{8}$$

where TSE_{jk} is the four-instrument variance that would be computed if the initial faulty instrument (j) and the new but unknown failed instrument (k) were omitted in the processing.

The failure-isolation algorithm implements these concepts in the following manner. First, all six individual errors are computed and Eq. 6 is used to calculate TSE_0. The total squared error is compared to an allowable threshold, which may be varied as a function of the mission requirement and dynamic environment. If the system is operating within the acceptable TSE_0 criteria, no further activity is required until the next failure-isolation iteration. If the TSE_0 criterion is violated, the ratio of each individual instrument

squared error is taken with respect to the TSE_0. If, for example, $E_a'^2$ is a significant percentage of TSE_0, failure of instrument A is indicated. The 50% criterion previously noted represents a theoretical upper limit since the use of quantized data and the instrument population's acceptable noise and residuals computationally increase all the E_j' terms and the TSE_0. Thus, if a 50% criterion is used, failures would go undetected. Similarly, the use of a very low percentage would result in false alarms. Our studies have shown that a ratio of 0.44 yields a highly-sensitive reliable failure-isolation capability in a realistic system implementation. A second failure is detected when the TSE_j criterion is exceeded. This failure is isolated by taking the ratio of $E_{jk}'^2$ to TSE_j, and for this case, the theoretical limit is 40% (Eq. 8).

The failure-isolation algorithm operates on measurement data that are iteratively accumulated by a low-pass digital filter. The filter time constant is selected to be consistent with the acceptable error resolutions and the filtering technique is used to minimize the noise effects resulting from the use of quantized data. Finally, after isolation of two failures, detection of a third is achieved by monitoring the single remaining parity equation (Table 2) that corresponds to the operational state of the system.

An example of the error detection process is shown for the SIRU system in Fig. 3. This figure shows a plot of the $E_j'^2$ magnitude (in pulses squared) for all instrument axes as a function of test time. A simulated failure is introduced in the A axis gyro (bias miscompensated by 25 meru after 120 sec of normal system operation). Note that the $E_a'^2$ error magnitude increases until the failure detection threshold is exceeded, 150 sec after the fault was introduced, and then the failure is isolated to the A gyro. After isolation, the A gyro data is not processed and the error propagation in the estimate of B through F instrument errors are reduced significantly. The resultant system-attitude error, during this time interval, Fig. 4, shows the gyro drift-rate error propagating as an attitude error until detection and isolation occur. The total error accumulation caused by this A gyro failure is less than 15 arc sec in both the X and Z axes. One should note that the fault detection is time-dependent since it is based on the magnitude of accumulated $E_j'^2$ pulses. Thus, the magnitude of attitude error is always bounded within 15 arc sec regardless of the magnitude of the instrument drift-rate error.

In the present implementation, the gyro failure-isolation criteria allow detection and isolation in 35 sec for a performance deterioration equivalent to a 100-meru change in bias. Similarly, an accelerometer bias change equivalent to a 0.1 cm/sec^2 can also be detected and isolated. Proportionately longer times would be required for detection of smaller performance changes. Equivalent detection and isolation is achieved for instrument-axis scale factor and alignment degradation.

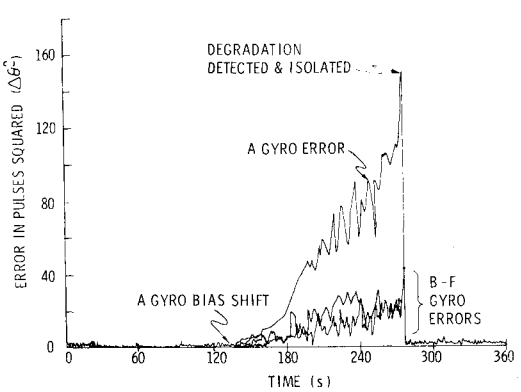

Fig. 3 Instrument squared error vs time for 25 meru BD shift in A gyro at 120 sec.

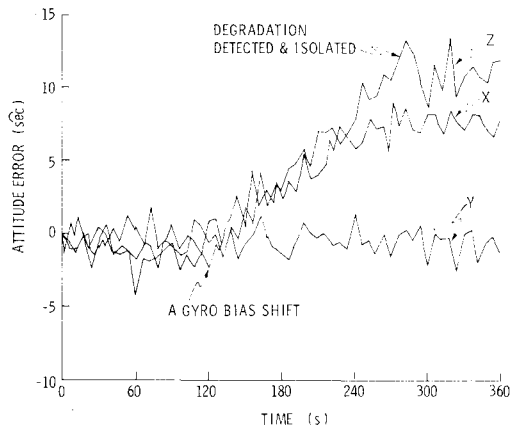

Fig. 4 Quaternion attitude error vs time for 25 meru bias shift in A gyro at 120 sec.

General-System Software Description

A general-purpose computer (Honeywell DDP-516) is used to verify the redundant SIRU system software design by providing an instrument calibration and real-time system evaluation capability. The DDP-516 is a 16-bit machine with memory cycle time of 0.96 μsecond, a high-speed arithmetic package, and 16,384 words of core memory. Peripherals used include: two disc drives, each capable of storing 34 million words; teletype unit; a CRT character display; and a high-speed paper-tape reader. The DDP-516 has been interfaced with the test table encoder as well as the SIRU instrument module outputs, and thereby provides a capability of real-time evaluation.

The present SIRU software mechanization is shown in Fig. 5. In this mechanization the torque-to-balance instrument loop delivers incremental information at a 4800-pps rate. The basic matrix processors and the attitude and velocity algorithms, may be operated at rates of 20 to 100-updates/sec. The velocity and attitude processing is done sequentially in each update interval and uses velocity and attitude data accumulations that are staggered by a half cycle. This permits the incremental acceleration accumulation to be processed into the inertial frame using the average attitude over the accumulation interval.

Each raw gyro and accelerometer data accumulation is compensated to account for the instrument control-loop errors. The compensating software routines generate corrections to the raw instrument-data accumulations by modeling the instrument-loop error sources and estimating each instrument's static and dynamic environment inputs. The coefficients of the error model and determined from a series of static and dynamic calibration tests. The error terms that are modeled are shown in Table 3. The update rate used for each correction term is tabulated along with its computer timing and memory requirements. Routines developed include compensation for gyro output-axis coupling (psuedo-coning drift)[4] and accelerometer rotational dynamics. Each correction is summed into each $\Delta\theta$ or ΔV instrument correction register at its respective update time. The summed corrections enter the matrix processors and failure-isolation algorithms as each correction register reaches its corresponding data quantization size.

Referring again to Fig. 5, the corrected incremental body motion and velocity information is first processed by the failure-isolation equations and, if no failure is detected, it is then processed by the appropriate least-square matrix. The output of the least-square processing is the reference-triad solution discussed previously. The failure-isolation processing, as explained, outputs TSE_0 and $E_J'^2/TSE_0$ ratios for comparison with the failure detection and isolation criteria. The failure processing and comparison occurs every

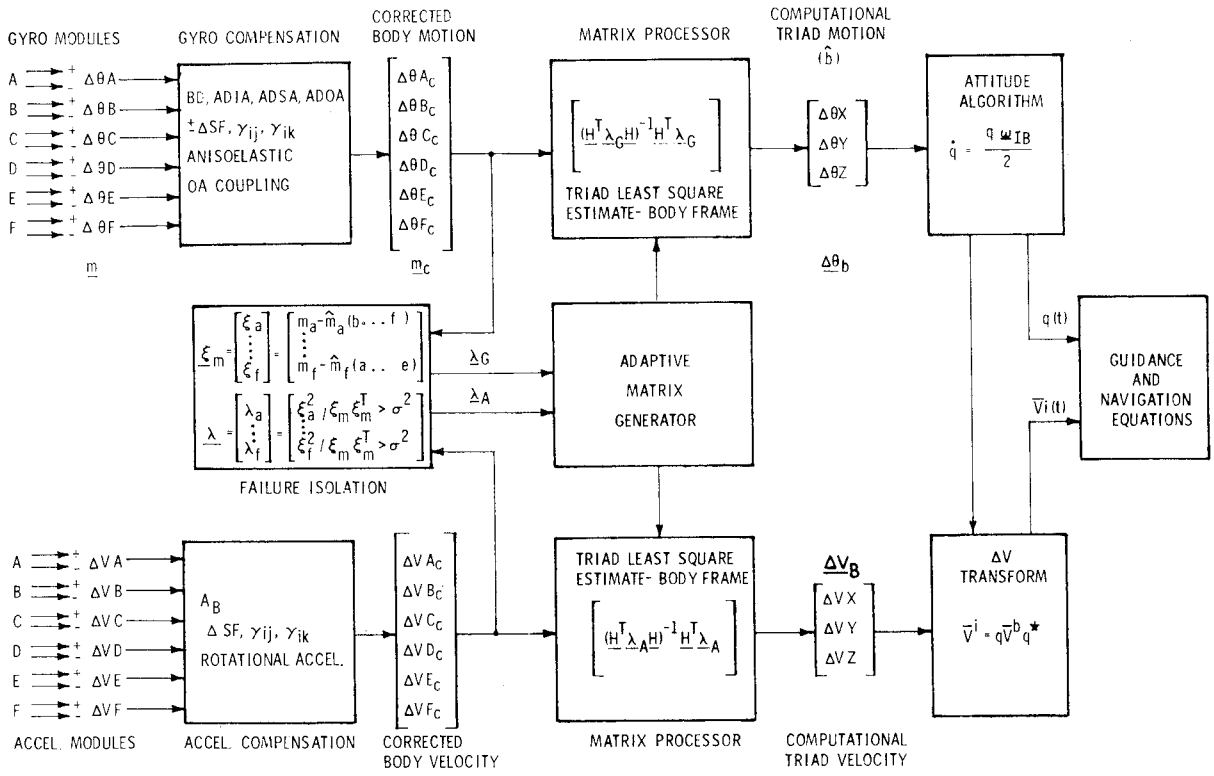

Fig. 5 SIRU data processing.

update interval. If a failure is detected and isolated, the failure state is entered into the adaptive matrix generator which reorganizes the matrix processor. The matrix generator can reorganize the processing matrices to account for all failure combinations within a reorganization time of 500 μseconds for a worst-case failure state.

The output of the matrix processors is used by the attitude and velocity algorithms. The attitude algorithm is a third-order quaternion of rotation.[5] A third-order Taylor series expansion is used to achieve high performance at low-iteration rates. The ΔV transformation derived from the quaternion attitude output is processed into a three-by-three direction-cosine transformation. An advantage in using a quaternion for this transformation is that perfect ΔV orthogonalization is assured by simply normalizing the quaternion single-length constraint. Further, use of the quaternion technique simplifies initial alignment and autopilot control[6] programs.

The complete software requirements for the system mechanization using a computational rate of 20 updates/sec is listed in Table 4. The total computational system is shown to require 16.3% of the available DDP-516 time. A comparable mechanization at a 100 update/sec computational rate would require 72.3% of the machine time.

Table 3 Instrument compensation subroutines

	Compensation rate (updates/sec)	Compensation Memory (words)	Compensation % Real-time consumed
Accelerometer processing			
Input read routine	20	30	0.1
Scale factor (average)	20	50	0.2
Misalignment (IA about PA and OA)	10	110	0.6
Bias	4	26	0.0
Generate ADIA, ADSA, ADOA	10	90	0.3
Anisoelastic	10	128	0.3
Compensation accumulator and correction	20	34	0.3
Total accel loop		468	1.8
Gyro processing			
Input read routine	20	30	0.1
Scale factor (+ and −)	20	80	0.2
Misalignment (IA about PA and OA)	10	110	0.6
Bias drift	4	26	0.0
OA coupling	20	105	0.3
Compensation accumulation and correction	20	34	0.3
Total gyro loop		385	1.5

Table 4 SIRU software requirements

	Memory (words)	% Real-time consumed
Accelerometer processing		
Coefficient compensation	468	1.8
Matrix processor	90	1.5
Failure isolation and adaptation	800	2.0
ΔV transformation	220	3.0
Total accel—subloop	1578	8.3
Gyro processing		
Coefficient compensation	385	1.5
Matrix processor	90	1.5
Failure isolation and adaptation	800	2.0
Attitude transformation	300	3.0
Total gyro—subloop	1575	8.0
SIRU DDP 516 requirements	3153	16.3

Electronics

Redundant Mechanization

The previous discussions developed SIRU's redundant data-processing and failure-isolation concepts. In this section, the manner in which the concepts are extended to the electronics are reviewed.

Redundant techniques are employed in the electronic mechanization to provide instrument-electronic functions that are free from single-point failure mechanisms. Figure 6 illustrates the basics of the mechanization. Functional axes have been defined that correspond to each dodecahedron measurement axis. Each axis consists of a gyro and an accelerometer module supported by common power supplies. These include: a 2-phase 800-Hz gyro-wheel power supply; a 9600-Hz supply for suspension and signal-generator excitation; and a d.c. axis supply. The d.c.-axis supply provides the modules' torque electronics with the required logic (5v) and amplifier ($\pm$10v) voltage levels and a floating excitation (15v) for each loop's precision-voltage reference. This per-axis implementation enables any singular computational isolation of any failure at either an instrument axis or, at worst, a functional axis level. The functional axis concept was implemented for ac and floating dc-power supplies since a dual-redundant implementation would have necessitated a complex and unreliable system of independent failure-detection monitors and switching networks. Each gyro and accelerometer module includes its own temperature controller, ternary torque-to-balance control loop, and other specialized instrument electronics.

The mechanization shown allows for the incremental $\Delta\theta$ and ΔV outputs of each instrument module to be stored redundantly in an interface multiplexer. The multiplexer would then transmit data and receive control and sampling messages from the computer assembly on dual buses. A serial data-transmission format would be used with provisions for transmission of digitized analog data (voltages, etc.) for automatic monitoring.

Redundant d.c.-power distribution to the functional axes is achieved by the use of dual d.c.-power supplies. These are designed so that each can independently support the total load of all functional axes. They are isolated from each other by diode networks to provide fail-safe operation.

Discussion of the dual 40V supply-design implementation, which provides power for the gyro torquing current, provides insight into the special design considerations that are applicable to avoid a system failure due to a single-point failure mechanism. First and most obvious, the diode interconnection is provided on a per-axis basis to assure the availability of 40V power to the gyro modules if either of the two supplies fail with a below-level output or an internal short circuit occurs preceding the diode. Similarly, to protect against a gyro-module short circuit, fusing is incorporated on a per-axes basis to assure the 40V distribution to all other gyro modules (a solid-state fuse design has been formulated). Another more subtle reliability design requirement becomes apparent when one notes that the 40V to the gyro-module torque loops must remain within regulation limits to prevent performance degradation on all axes. Therefore, each 40-volt module has dual-redundant feedback loops that regulate and limit its maximum output voltage. Other design features allow a 100% continuous overload and a 50% underload (operation with as few as three gyro-modules) without affecting regulation and system performance.

The timing control pulses for the torque electronics and the synchronization functions for the various power supplies are also redundantly implemented. The oscillators are mechanized in a triple-redundant configuration with output-frequency comparisons and individual failure detectors.

Dual redundancy is employed in the scaler implementation and high/low frequency detectors test both the 115.2-kpps and 200-pps outputs. The control pulses to the torquing electronics are also tested for their presence and sequence. The selection logic gates only one scaler at a time to the system functional axes and power supplies, while both scalers are continuously operated and monitored by their detectors. The scaler-output lines are separately buffered to assure fail-safe operation. In both the scaler and oscillator implementation provisions for test sequencing of the combinations are included.

It is important to note that the electronic-system configuration has been mechanized to provide fail-safe isolation characteristics. The degree of redundancy used was also based on the relative reliability of the particular functional elements. For example, the estimated failure rate of a 40V power supply is less than 10 per million hr while a gyro-module failure rate estimate might range between 100 and 200 per million hr, dependent upon the instrument and torque electronics. Thus, for the d.c.-power supply, dual

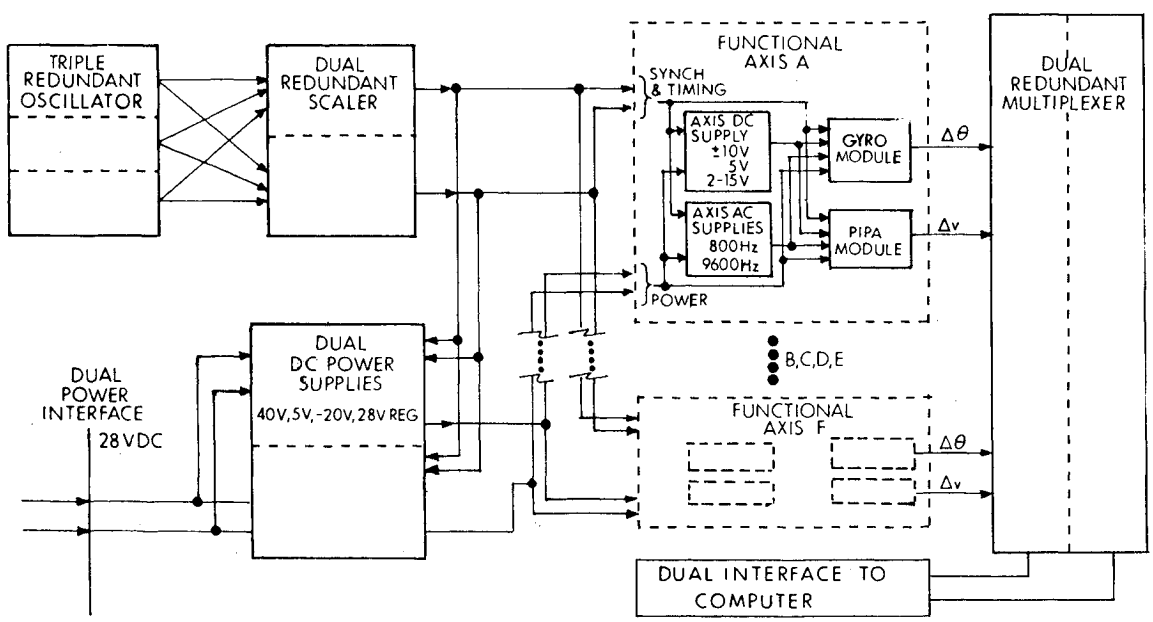

Fig. 6 Block diagram of SIRU inertial component sensor assembly.

redundancy is sufficient and does not compromise the end-to-end system reliability index.

Module Electronics

As noted, each gyro and accelerometer module includes its own temperature controller, preamplifier, torque control loop, etc. Scale-factor stability and linearity performance on the order of 10 and 50 ppm, respectively,[7] is achievable with the present instrument control-loop out to a 1 rad/sec torque-loop design range.

A functional block diagram of the gyro module is shown in Fig. 7. Note that an interpolator/compensator has been added to the ternary-torque-to-balance loop function.

In standard ternary-loop operation, the gyro-signal generator (SG) output is sampled and, when the SG signal reaches a given threshold, the control logic applies a torque-current pulse to the gyro-torque generator to return the gyro float to its null position. Timing pulses to the logic control the current-pulse width while precision current-amplitude control is effected by a current feedback loop that operates on the basis of a comparison between a precision-voltage reference and a current sampling resistor. The interpolator/compensator provides a dual function. The compensator[8] corrects for the dynamic storage characteristic of the gyro-float time constant and the interpolator samples float motion within the torque-loop control region to provide finer incremental angular measurements for improved computational algorithm performance. With respect to the compensator function, it linearizes the gyro-torque-loop output response to applied input rates. Ordinarily, due to the gyro's lagged float response to a torque pulse, moding or multiple pulsing with different on-off ratios at different input rates would occur. The compensator minimizes this effect by modeling the gyro's response and, based upon the torque-pulse commands, continuously developing a correcting signal that is summed with the gyro SG signal. A resultant linearized pulse-output response for input rates is then achieved by feeding this compensated signal to the torque-loop control logic.

The torquer compensation module includes RC networks that tune the torquer so that it is a resistive load for the current switch and a trim resistor for the "dummy" TG load. Since a ternary torque-loop is used, when torque is not required the current is applied to a "dummy" heater (equal in resistance to the torquer) on the gyro TG alignment end mount. This minimizes switching transients in the current control loop and applies constant power to the TG end of the gyro to minimize thermal gradients. The 8V power supply is located within the module to minimize lead capacitance which affects switching time in the current switch.

Table 5 Instrument torque-loop characteristics

A) Gyro torque loop:	
Type:	Linearized ternary-pulse torque-to-balance
Dynamic range:	1 rad/sec
Torque-loop quantization:	44 arc sec/pulse
Interpolator quantization:	5 arc sec/pulse
Torquer power:	2.94 watts—1 rad/sec
B) Accelerometer torque loop:	
Type:	Ternary pulse-torque-to-balance
Dynamic range:	19 g
Torque-loop quantization:	4 cm/sec per pulse
Torquer power:	0.78 watt—19 g's

A d.c. temperature control loop is used in the gyro and accelerometer modules. It is novel in that control power includes the output transistor's dissipation. The applied power therefore is a linear function of control current and a more efficient power mechanization also results. This is achieved by mounting the output power transistor on the instrument alignment mounts with the heater.

The accelerometer-module electronic configuration is similar to the gyro, except that the interpolator/compensator function is not used. The SIRU torque-loop scaling characteristics are listed in Table 5.

Packaging and Hardware

The packaging configuration that has been developed for the system embodies its reliability features in a modular implementation for improved maintainability. The system is configured as two separable assemblies: the inertial-sensor package, and its electronics assembly.

The Redundant Instrument Package consists of a mounting and alignment structure, commonly referred to as the π-frame, upon which the six gyro and six accelerometer modules mount. The assembled instrument package is shown in Fig. 8.

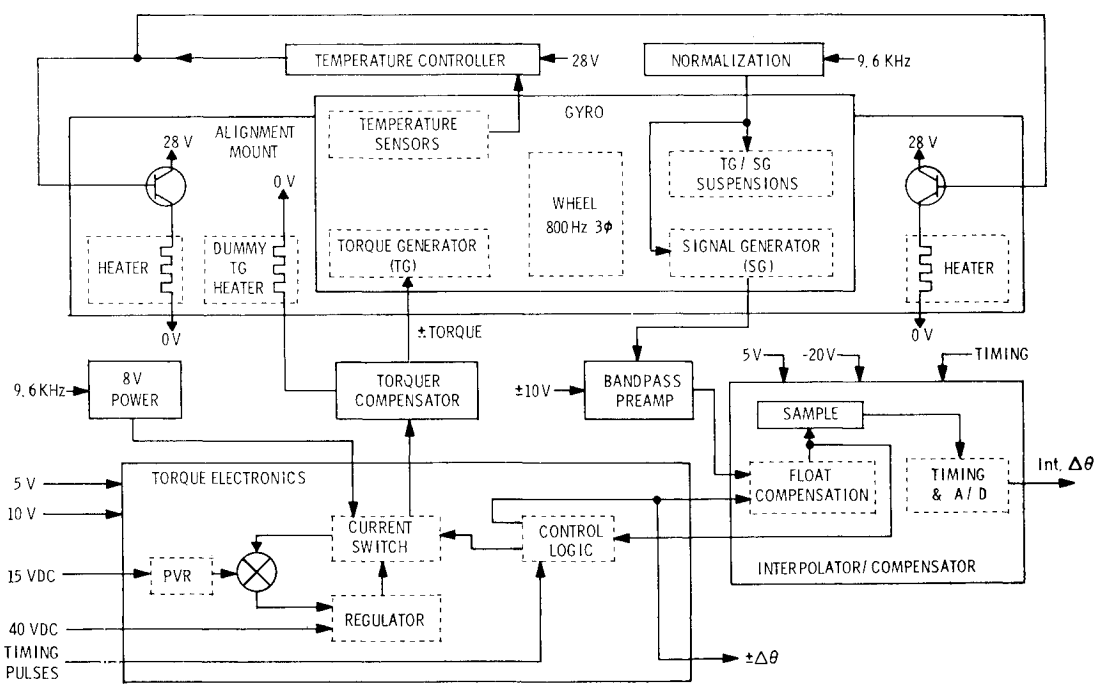

Fig. 7 A functional block diagram of the gyro module.

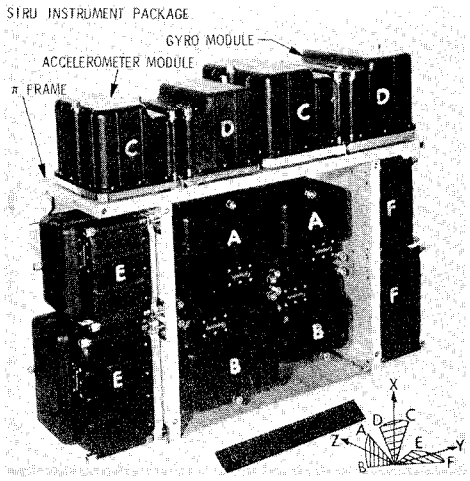

Fig. 8 SIRU instrument package.

Each module corresponds to a prealigned gyro or accelerometer that is normalized and packaged with its calibrated electronics in a sealed unit. The instrument input axis is offset at an angle, α, with respect to its module base. Thus, when the modules are mated with the π-frame's precision mounting surfaces, which lie in orthogonal planes, the instrument input axes are aligned to the desired dodecahedron symmetry. This mounting configuration allows all units to be prealigned in exactly the same manner and each type module is replaceable and interchangeable. Alignment offsets from module instrument alignment to system measurements after mounting on the π-frame have averaged less than 15 arc sec. Maintenance is further enhanced by the π-frame configuration that allows direct access to every instrument from the front of the package.

One interesting aspect of this mechanical configuration is that all instrument output axes are colinear with the reference orthogonal triad. This allows instrument output-axis dynamic corrections to be made on the basis of the triad solutions (Eq. 1) without additional geometric resolution.

The accelerometer module has been designed about the MIT-developed size 16 Pulsed Integrating Pendulous Accelerometer, a single degree-of-freedom specific-force receiver operated in a torque-to-balance mode. It is primarily distinguished from its predecessor, the Apollo PIPA, by a permanent-magnet torquer and a solid float.

The gyro module is designed about the size 18 Inertial Rate Integrating Gyroscope MOD B (18 IRIG),[9] a single degree-of-freedom gyroscope developed by MIT/DL. It is specifically designed for strapdown environment applications. Its permanent-magnet torquer is scaled for torque-to-balance

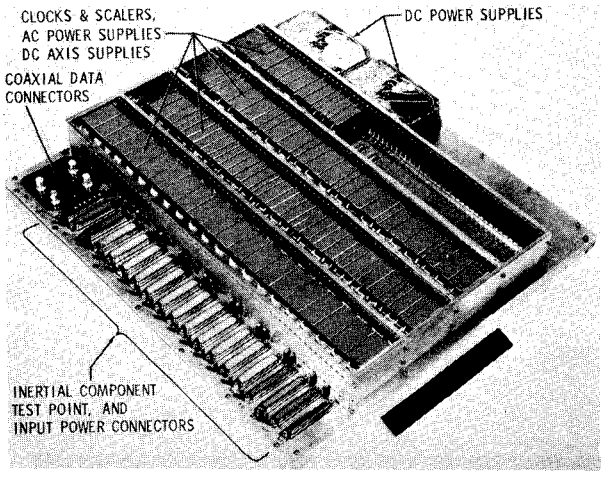

Fig. 9 SIRU electronics assembly.

Table 6 SIRU weight, power, and volume

Assembly	Weight (lb)	Volume (in.^{3})	Power (watts)
Redundant instrument package (RIP)	62.94	1753.84	182.4
Electronics assembly (EA)	33.5	1155.00	124.0
RIP—EA harness	6.25	—	—
Totals	102.7	2908.84	306.4

Table 7 Redundant instrument package

Assembly	Qty	Dimensions (in.)	Weight (lb)	Power (watts)
Gyro module	6	5-1/4×4-3/8×4	4.35	23.0
Accelerometer module	6	4-1/4×3-7/8×3-9/16	2.64	7.4
π-frame	1	20-1/4×15-1/16×5-3/4	21.00	—

operation with input rates of one radian per second and its suspension prevents radial side loading at this rate. It contains a gas-bearing wheel package, with a 5 rad/sec slew and multiple stop/start capability.

The packaging system developed by the U.S. Naval Avionics Facility, Indianapolis (NAFI) is used as the basis for the Electronics Assembly, shown in Fig. 9. It was selected because it expedited packaging since definition of the assembly structural design was possible prior to completion of all electronic module design and packaging. The *EA* design was configured so that functional redundant elements are mechanically and electrically separable. Thus, an oscillator module or portions of a scaler, etc., may be removed without disabling the system.

Weight, Volume, and Power

The Redundant Instrument Package and Electronic Assembly weight, volume, and power are itemized in Table 6. These data correspond to a packaging effort in which electronic microminiaturization development or special material selection to minimize weight were not pursued. A further itemization of the Redundant Instrument Package is shown in Table 7.

The SIRU configuration can be compared with the Apollo Inertial Subsystem (ISS) which has similar packaging density. The total Apollo equivalent ISS weight, volume, and power is 93 lbs, 2654 in.^{3}, and 216 watt. To achieve the same relative reliability as SIRU, three to four such systems would be required. (The Apollo IMU uses a larger size gyro; however, this is offset by the additional electronics, harnesses, and common navigational-base structure that would be required to achieve a fully redundant implementation.)

Conclusions

The nonorthogonal dodecahedron sensor array's characteristics allowed the development of a redundant system with minimum error propagation under failure conditions using self-contained techniques that isolate up to two failures of either instrument type and continued operation with three failures.

It has been shown that a deterministic failure-isolation and adaptation method is efficiently integrated in a complete operating system and has been demonstrated with a DDP-516 test-evaluation computer.

The added reliability attained using the dodecahedron concept has been complemented by the redundant electronics

which is mechanized to free this system from the possibility of system failure from single-point failure mechanisms.

The modular instrument configuration provides an isolated instrument control-loop function that is an efficient subset for assembly, normalization, and test, and enhances reliability. This mounting configuration allows a high-density instrument package in which all of the modules are readily accessible for replacement and maintenance.

Some areas still under study include system miniaturization using hybrid packaging with smaller size 13 instruments and self-calibration of instruments in operational phases using the redundant data.

References

[1] Gilmore, J. P., "A Non-Orthogonal Gyro Configuration," MIT/IL Rept. T-472, Jan. 1967, MIT, Cambridge, Mass.

[2] Crisp, R., Gilmore, J. P., and Hopkins, A. L., "SIRU—A New Inertial System Concept for Inflight Reliability and Maintainability," MIT/IL Rept. E-2407, May 1969, MIT, Cambridge, Mass.

[3] Ephgrave, J. T., "Redundant Adaptive Strapdown Inertial Navigation System," Rept. TOR-0066(5306)-10, Oct. 1969, Aerospace Corp., El Segundo, Calif.

[4] Gilmore, J. P. and McKern, R. A., "Strapdown Inertial Attitude-Indication Evaluations," *Journal of Spacecraft and Rockets*, Vol. 7, No. 7, July 1970, pp. 825–831.

[5] McKern, R. A., "A Study of Transformation Algorithms for Use in Digital computer," MIT/IL Rept. T-493, Jan. 1968, MIT, Cambridge, Mass.

[6] Ickes, B. P., "A New Method for Performing Digital Control System Attitude Computations Using Quaternions," *AIAA Journal*, Vol. 8, No. 1, Jan. 1970, pp. 13–17.

[7] Feldman, J., and Gilmore, J. P., "The Gyroscope in Torque-to-Balance Strapdown Application," MIT/IL Rept. E-2392, April 1969, MIT Cambridge, Mass.

[8] Lory, C. B., Compensation of Pulse Rebalanced Inertial Instruments, MIT/IL Rept. T-495, Jan. 1968, MIT, Cambridge, Mass.

[9] FBM/IC Staff, 18 IRIG Mod B 420 Series Final Report, MIT/CSDL Rept. R-664, June 1970, MIT, Cambridge, Mass.